Solar Energy Materials & Solar Cells 109 (2013) 77–81

Contents lists available at SciVerse ScienceDirect

Solar Energy Materials & Solar Cells

journal homepage: www.elsevier.com/locate/solmat

Spatially resolved photoluminescence imaging of essential silicon solar cell parameters and comparison with CELLO measurements

Chao Shen [a,*], Henner Kampwerth [a], Martin Green [a], Thorsten Trupke [a], Jürgen Carstensen [b], Andreas Schütt [b]

[a] University of New South Wales, Sydney, NSW 2036, Australia
[b] Christian-Albrechts-Universität zu Kiel, Kaiserstrasse 2, Kiel 24143, Germany

ARTICLE INFO

Article history:
Received 5 July 2012
Received in revised form
28 September 2012
Accepted 8 October 2012
Available online 16 November 2012

Keywords:
Solar cells
Luminescence
Photoluminescence
Spatially resolved
Efficiency map
Current map

ABSTRACT

We present a method to image the following parameters spatially resolved of a solar cell: voltage V_{xy}, current density J_{xy}, power density P_{xy}, efficiency η_{xy}, series resistance $R_{s,xy}$, fill factor FF_{xy} and dark saturation current densities of a two diode model $J_{01,xy}$ and $J_{02,xy}$. The algorithm determines this set of self-consistent parameters by using a minimum of 5 electrical biased photoluminescence images. A comparison with CELLO measurements supports the presented method.

1. Introduction

In recent years, several publications [1,2,4,6–11] focused on the extraction of spatially resolved maps of electrical parameters from photoluminescence (PL) images, after Trupke et al. [12] found the large area PL imaging technique. The majority of the methods [4,6–8] require a local calibration constant C_{xy} that is calculated in an individual step with its own PL images. This and associated assumptions for C_{xy} may create an inconsistent set of result parameters/maps. Kampwerth et al. [1] could avoid the use of C_{xy} completely, but their method is limited to the calculation of the local series resistances $R_{s,xy}$ and could not be further extended. The work of Glatthaar et al. [2] calculated C_{xy} together with the local voltage V_{xy} and dark saturation current density $J_{0,xy}$ by using a one diode model. With this, they created a self-consistent set of output parameters. Our method follows Glatthaar's lead and extends it to more parameters. Also, compared to the work published in IEEE conference [3], additional comparison with CELLO measurements will be discussed.

2. The algorithm

Our algorithm uses a minimum of 5 PL images at different electrical bias and illumination conditions. The principle data flow is shown in Fig. 1. In this context, subscript xy are the coordinates of a point on the cell, and all the maps are calculated point by point.

The commonly accepted correlations between luminescence photon flux $\phi_{PL,xy}$ (i.e. PL images) and the local voltage V_{xy} [4,13] are reflected in Eqs. (1) and (2a). C_{xy} is the calibration constant and assumed to be independent of electrical bias or illumination conditions. Eq. (2a) calculates the net PL photon flux $\phi_{net,xy}$ that is used in Eq. (1). Eq. (2b) is Glatthaar et al.'s [2] approximation that only one image $\phi_{offset,xy,1\ sun}$ at short circuit and 1 sun illumination condition is required to determine the offset photon flux $\phi_{offset,xy}$ primarily caused by diffusion limited carrier recombination [4]. To calculate $\phi_{offset,xy}$ at different illumination intensities, a scaling factor I_{sun} is used. It is the dimensionless fraction of a 1 sun equivalent photon flux and scales the offset PL photon flux at 1 sun equivalent $\phi_{offset,xy,1sun}$. The thermal voltage $V_T = kT/q$. The local current density J_{xy} is defined by the common two-diode model without shunt [5], see Eq. (3). The light generated current density J_{light} is assumed to be uniform throughout the cell and equals to its short circuit current density J_{sc}. Eq. (4) describes the current density J_{xy} that is defined by the voltage drop between the local voltage V_{xy} and terminal V_{term} on the local series resistance $R_{s,xy}$:

$$V_{xy} = V_T \ln\left(\frac{\phi_{net,xy}}{C_{xy}}\right) \tag{1}$$

$$\phi_{net,xy} = \phi_{PL,xy} - \phi_{offset,xy}, \tag{2a}$$

* Corresponding author. Tel.: +61 433666505.
E-mail address: hunterchaoshen@gmail.com (C. Shen).

0927-0248/$ - see front matter Crown Copyright © 2012 Published by Elsevier B.V. All rights reserved.
http://dx.doi.org/10.1016/j.solmat.2012.10.010

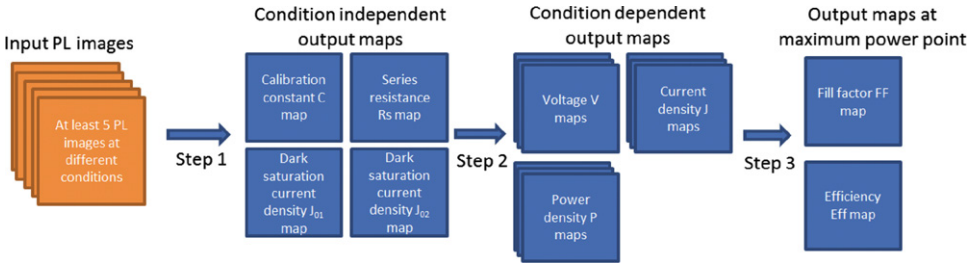

Fig. 1. Flow chart of the method. With a minimum of 5 input PL images, the 1st step calculates the condition independent output maps. The 2nd step calculates condition dependent output maps. The output maps in this step vary with different conditions. The 3rd step calculates the maps at maximum power point condition only.

with

$$\phi_{\text{offset},xy} = I_{\text{sun}}\,\phi_{\text{offset},xy,1\ \text{sun}}, \tag{2b}$$

$$J_{xy} = -J_{01,xy}\left(e^{v_{xy}/v_T}-1\right) - J_{02,xy}\left(e^{v_{xy}/2v_T}-1\right) + J_{\text{light}} \tag{3}$$

$$J_{xy} = \frac{V_{xy} - V_{\text{term}}}{R_{S,xy}} \tag{4}$$

$$\underbrace{V_T \ln\left(\phi_{net,xy}\right) - V_{term}}_{a_{xy}} = \underbrace{V_T \ln C_{xy}}_{W_{xy}} + \underbrace{R_{S,xy}}_{X_{xy}}\underbrace{J_{light}}_{b_{xy}}$$
$$\underbrace{-\frac{J_{01,xy}R_{S,xy}}{C_{xy}}}_{Y_{xy}}\underbrace{\phi_{net,xy}}_{C_{xy}} \underbrace{-\frac{J_{02,xy}R_{S,xy}}{\sqrt{C_{xy}}}}_{Z_{xy}}\underbrace{\sqrt{\phi_{net,xy}}}_{d_{xy}} \tag{5}$$

The upper half of Eq. (5) is found by combining Eqs. (1), (3) and (4).

As shown in Fig. 1, the algorithm consists of 3 major steps. The first step has two options, A and B.

Step 1:

Option A with 5 input images

The lower half of Eq. (5) substitutes sections of the upper equation into knowns a_{xy}, b_{xy}, c_{xy} and d_{xy} and unknowns W_{xy}, X_{xy}, Y_{xy} and Z_{xy}. Each PL image i generates one set of known values $a_{i,xy}$, $b_{i,xy}$, $c_{i,xy}$ and $d_{i,xy}$. The resulting linear equation therefore requires 4 PL images at different conditions (electrical bias and illumination intensity) to solve for the four unknowns. To calculate net photon flux $\phi_{\text{net},xy}$ in Eq. 2, a fifth image $\phi_{\text{offset},xy,1\ \text{sun}}$ is also needed.

Option B with more than 5 input images

Eq. (5) can also be solved by more than 5 images via a linear regression fit. Each PL image will generate one set of variables $a_{i,xy}$, $b_{i,xy}$, $c_{i,xy}$ and $d_{i,xy}$, which are the coordinates of a point in a four dimensional (4D) space. All images will ideally generate points on a single line in this 4D space. The linear regression is a least square fit to find the most agreeable line for all the points. The number of input PL images is therefore flexible, as long as more than 5 images are used. A higher number of input images will reduce the resulting uncertainty and noise of the final output parameters.

Once the unknowns W_{xy}, X_{xy}, Y_{xy}, and Z_{xy} are found, either via option A or B, the cell's parameters can be calculated by the substitutions in Eq. (5). See below:

$$C_{xy} = e^{W_{xy}/V_T} \tag{6a}$$

$$R_{S,xy} = X_{xy} \tag{6b}$$

$$J_{01,xy} = Y_{xy}\frac{C_{xy}}{R_{S,xy}} \tag{6c}$$

$$J_{02,\,xy} = Z_{xy}\frac{\sqrt{C_{xy}}}{R_{S,xy}} \tag{6d}$$

Step 2:

The parameters in step 1 are assumed to be independent of the electrical bias and illumination conditions, while local voltage V_{xy}, current density J_{xy}, and power density P_{xy} are dependent on these conditions. In the second step, parameter maps can be calculated for arbitrary operating conditions. To analyze V_{xy}, J_{xy} and P_{xy} at a desired level of illumination and electrical bias, a PL image at this desired condition is required (This image could be the same as one of the input images in Fig. 1).

The local voltage V_{xy} can be calculated via Eqs. (1) and (2a) and (2b) by a PL image at the desired condition. For example, voltage image $V_{\text{oc},xy}$ at terminal open circuit condition is calculated via Eqs. (1) and (2a) and (2b) by a PL image at 1 sun and terminal open circuit condition.

The local current density J_{xy} and the effective usable local power density P_{xy} can be calculated via Eqs. (3) and (7) respectively for a desired operating condition:

$$P_{xy} = V_{\text{term}}\,J_{\text{xy}} \tag{7}$$

Step 3:

The power density map P_{xy} in unit mW/cm^2 can also be read as an efficiency map η_{xy} with 100 mW/cm^2 being 100% efficiency, if illumination equals to 1 sun equivalent (100 mW/cm^2) and the cell terminal is biased to maximum power point (MPP) voltage.

The same operating condition is used to calculate the fill factor FF_{xy} via

$$FF_{xy} = \frac{V_{\text{term}}J_{\text{xy}}}{J_{\text{sc}}V_{\text{oc},xy}} \tag{8}$$

3. Results

The following images are calculated by using 23 input PL images. The 5th image in step1 option A is taken at short circuit and 1 sun illumination condition. For the other 22 images, their electrical biases were varied from 490 mV (terminal MPP) to 700 mV and the illuminations were varied between 0.2 and 1 sun. All displayed images are from the same multi-crystalline solar cell.

The maps in Fig. 2 show the series resistance of each pixel $R_{s,xy}$ toward the cells terminal. The local dark saturation current density $J_{01,xy}$ is shown in Fig. 3a. It is a good descriptive parameter for the bulk recombination characteristics. The local dark saturation current density $J_{02,xy}$, Fig. 3b, represents the junction recombination characteristics together with some other efficiency reducing effects. The distribution of the simultaneously calculated

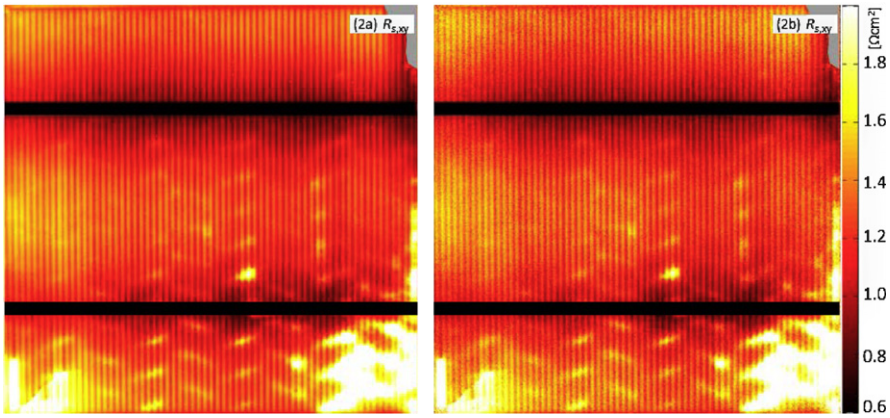

Fig. 2. Comparison of series resistance maps $R_{s,xy}$ calculated independently by two algorithms. (2a) The new method—To reduce noise, 23 PL images were used. The series resistance is low in the regions close to busbars and high at the crack (bottom left) and the belt print regions. (2b) Method of Kampwerth et al. [1], which is used by BT-imaging [14]. Six input images were used. Both maps agree within 5% of individual values and show the same features.

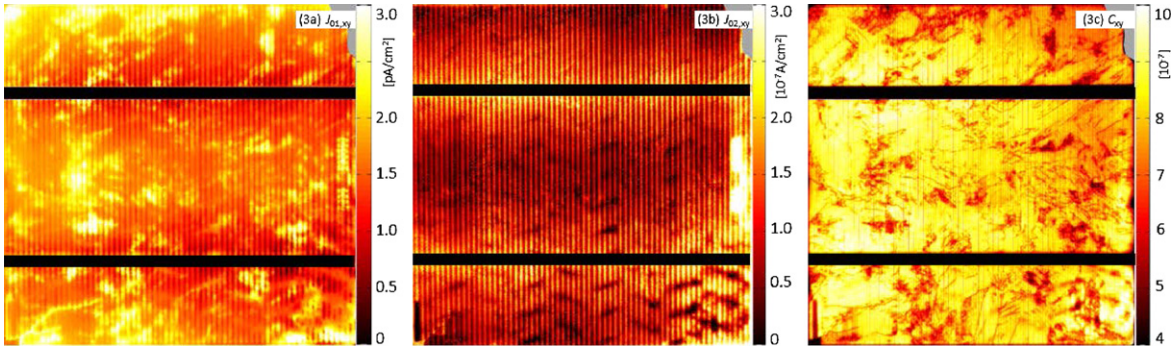

Fig. 3. (3a) Dark saturation current density $J_{01,xy}$ map. The multiple regions of high J_{01} values are likely caused by low lifetime at grain boundaries. (3b) Dark saturation current density $J_{02,xy}$ map. The high value of J_{02} in mid-right region (boxed) of the cell is likely caused by high junction recombination. (3c) Calibration constant map C_{xy}. Values are influenced by various optical and electrical properties of the cell.

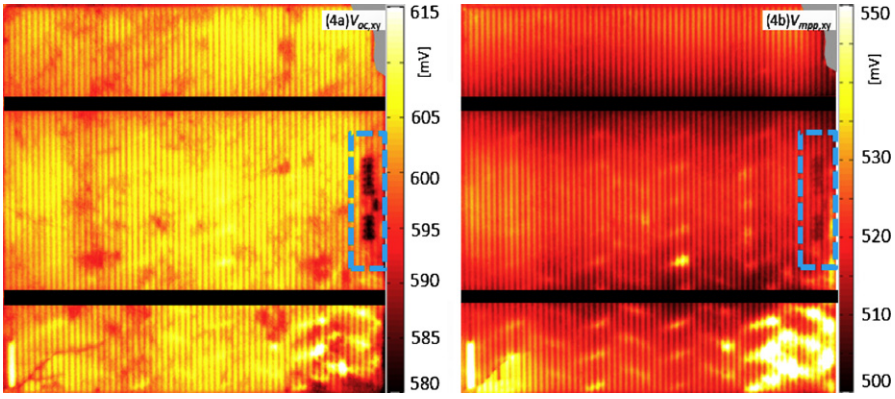

Fig. 4. Voltage maps. (a) Voltage map $V_{oc,xy}$ at terminal open-circuit. The low voltage area located to the mid-right of the cell is caused by high $J_{02,xy}$ values, see Fig. 3(b). 4(b) Voltage map $V_{mpp,xy}$ at terminal maximum power point. The pattern is dominated by the series resistance, see Fig. 2(a). Only the pattern in the right region differs markedly from Fig. 2(a).

local calibration constant C_{xy} in Fig. 3c is required in Eqs. (2a) and (2b). The local junction voltage V_{xy} at 1 sun illumination and open circuit voltage is shown in Fig. 4a, and at maximum power point in Fig. 4b.

Fig. 5a shows the local current generation J_{xy} toward the cells contacts. The fill factor map FF_{xy} is shown in Fig. 5b. Fig. 5c presents the distribution of the electrical power density P_{xy} generated by each pixel at 1 sun illumination and terminal MPP. At this operating condition the same map in mW/cm^2 is also the conversion efficiency distribution map with values in %.

4. Comparison with CELLO measurements

The experimental results were compared with measurements by CELLO (solar CELl Local characterization) [15], which is

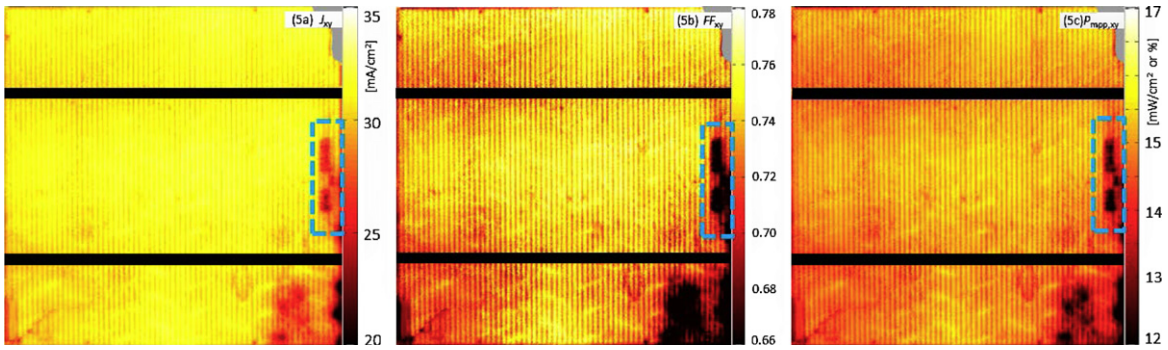

Fig. 5. (a) Current density map J_{xy} at terminal maximum power point and 1 sun equivalent illumination. It can be seen that mid right and bottom right regions of the cell have low current output, which are likely caused by high junction recombination and high resistance respectively. This map seems to be correct as the current sum of all the local points matches the measured global current at the terminal. 5(b) Fill factor map FF_{xy}. 5(c) Power density map P_{xy} at terminal maximum power point and 1 sun equivalent illumination. It is equivalent to an efficiency map [%]. The majority of points have an efficiency of 15.5%, while the mid right and bottom right regions have an efficiency of less than 14%.

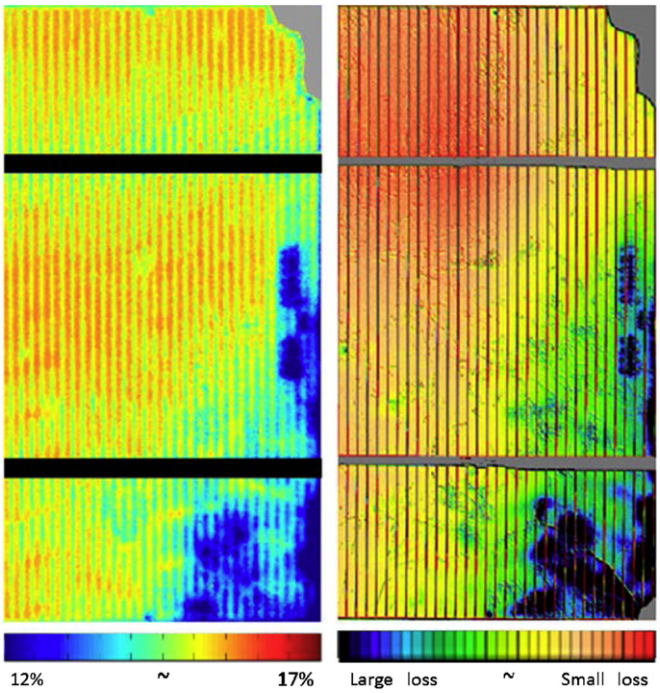

Fig. 6. The comparison of the efficiency map by the new method (left) and power loss map by CELLO (right). The crack and missing corner on the bottom right in the right map is caused by shipping breakage.

commonly known as a comprehensive high resolution mapping tool for solar cells characterization.

CELLO provides maps of different solar cell parameters by analyzing the linear small signal response in current or voltage due to a local perturbation, i.e. illumination by a laser beam per cell. One IV curve and four current and voltage maps (resolution around 1000 pixel $\times$ 1000 pixel) at different points along the IV curve under 0.3 sun global bias light illumination were measured and used for the calculation of various cell parameter maps like series resistance. As expected, all maps of the same parameter show very good agreement with the new method, e.g. the overall efficiency map showed almost the same features as the power loss map by CELLO measurements, see Fig. 6. There was no hint found in the CELLO results that the new method is not correct. As be illustrated by the laser scribing marks (numbers on right cell's side in Fig. 6) the CELLO method reveals clearer details of the defect distribution, while the corresponding new method's image is more blurred. This is caused by systematic differences in the measurement principle between CELLO and PL, i.e. basically how local currents and voltages at each pixel are generated, distributed and controlled.

However, the new method is much faster (around 1–2 min totally for 9 images, compared to around 2.5 h for the 4 CELLO maps) and gives self-consistent quantitative values.

5. Conclusion

A method is presented to calculate a complete and consistent set of performance parameter maps. Five or more images can be used, while more images will reduce the residual noise. In extension to other publications [1,2,4,6–10], additional maps of dark saturation current densities of a two diode model, current density, power density, fill factor and efficiency are calculated. Furthermore, no assumptions are used for the commonly needed local calibration constant. The calculated parameter set is self-consistent. All the

output parameters are effective values, valid at homogeneous illumination condition, which reflect well the intended operating condition of solar cells. A comparison with CELLO agrees with the features of the individual parameter maps.

References

[1] H. Kampwerth, T. Trupke, et al., Advanced luminescence based effective series resistance imaging of silicon solar cells, Applied Physics Letters 93 (202102) (2008) 202103.

[2] M. Glatthaar, J. Haunschild, et al., Evaluating luminescence based voltage images of silicon solar cells, Journal of Applied Physics 108 (2010) 014501.

[3] C. Shen, H. Kampwerth, et al., Spatially resolved photoluminescence imaging of essential silicon solar cell parameters, in: Proceedings of the 38th IEEE Photovoltaic Specialists Conference, Austin, USA, 2012.

[4] T. Trupke, E. Pink, et al., Spatially resolved series resistance of silicon solar cells obtained from luminescence imaging, Applied Physics Letters 90 (2007) 093506.

[5] M. Wolf, H. Rauschenbach, Series resistance effects on solar cell measurements, Advanced Energy Conversion 3 (2) (1963) 455–479.

[6] D. Hinken, K. Ramspeck, et al., Series resistance imaging of solar cells by voltage dependent electroluminescence, Applied Physics Letters 91 (2007) 182104.

[7] O. Breitenstein, A. Khanna, et al., Quantitative evaluation of electroluminescence images of solar cells, Physica Status Solidi (RRL)—Rapid Research Letters 4 (2010) 7–9.

[8] M. Glatthaar, J. Haunschild, et al., Spatially resolved determination of dark saturation current and series resistance of silicon solar cells, Physica Status Solidi—Rapid Research Letters 4(Compendex) (2009) 13–15.

[9] J. Haunschild, M. Glatthaar, et al., Fast series resistance imaging for silicon solar cells using electroluminescence, Physica Status Solidi (RRL)—Rapid Research Letters 3 (7-8) (2009) 227–229.

[10] M. Kasemann, D. Grote, et al., Luminescence imaging for the detection of shunts on silicon solar cells, Progress in Photovoltaics: Research and Applications 16(Compendex) (2008) 297–305.

[11] C. Shen, H. Kampwerth, et al., Luminescence based efficiency and other important parameters imaging of silicon solar cells, in: Proceedings of the 27th EU-PVSEC Conference, Messe Frankfurt, Germany, 2012.

[12] T. Trupke, R.A. Bardos, et al., Photoluminescence imaging of silicon wafers, Applied Physics Letters 89 (2006) 044107.

[13] T. Fuyuki, H. Kondo, et al., Photographic surveying of minority carrier diffusion length in polycrystalline silicon solar cells by electroluminescence, Applied Physics Letters 86(Compendex) (2005) 1–3.

[14] BT Imaging Pty Ltd. 〈http:www.btimaging.com〉.

[15] J. Carstensen, A. Schütt, et al., CELLO local solar cell resistance maps: modeling of data and correlation to solar cell efficiency, in: Proceedings of the 22nd European Photovoltaic Solar Energy Conference, 1CV.1.34, Milan, 2007.